THE JOURNAL OF PHYSICAL CHEMISTRY B

Article

pubs.acs.org/JPCB

Dynamic Nuclear Polarization of ^{17}O: Direct Polarization

Vladimir K. Michaelis, Björn Corzilius,[†] Albert A. Smith,[‡] and Robert G. Griffin*

Francis Bitter Magnet Laboratory and Department of Chemistry, Massachusetts Institute of Technology, Cambridge, Massachusetts, 02139, United States

Supporting Information

ABSTRACT: Dynamic nuclear polarization of ^{17}O was studied using four different polarizing agents: the biradical TOTAPOL and the monoradicals trityl and SA-BDPA, as well as a mixture of the latter two. Field profiles, DNP mechanisms, and enhancements were measured to better understand and optimize directly polarizing this low-gamma quadrupolar nucleus using both mono- and biradical polarizing agents. Enhancements were recorded at <88 K and were >100 using the trityl (OX063) radical and <10 with the other polarizing agents. The >10 000-fold savings in acquisition time enabled a series of biologically relevant small molecules to be studied with small sample sizes and the measurement of various quadrupolar parameters. The results are discussed with comparison to room temperature studies and GIPAW quantum chemical calculations. These experimental results illustrate the strength of high field DNP and the importance of radical selection for studying low-gamma nuclei.

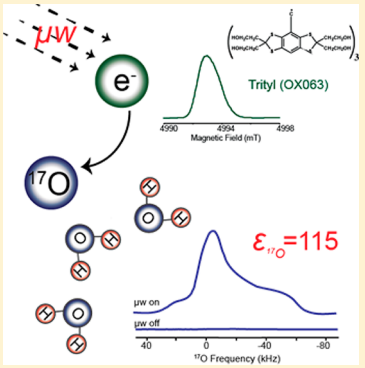

1. INTRODUCTION

Over the past few decades, a number of new methods and technologies have been developed to boost sensitivity and resolution in solid-state NMR experiments, for example, Hartmann−Hahn cross-polarization,[1] magic-angle spinning (MAS),[2,3] innovative methods for decoupling,[4−7] and high magnetic fields (≥16.4 T). These improvements have in turn enabled structural studies of peptides,[8] membrane,[9−12] and amyloid proteins[13−17] which would not be possible using conventional solution-state NMR or diffraction methods. Thus, it is now routine to examine ^{13}C, ^{15}N, and ^{31}P spectra and to measure distances and torsion angles that lead to molecular structures. More recently, the ability to extensively ^{2}H label proteins together with back exchange of the amide NH's and the availability of probes that spin at $\omega_r/2\pi \geq 65$ kHz have made detection of ^{1}H MAS spectra possible.[18−21]

In contrast, NMR studies of oxygen, the other copious element in biological systems, have progressed slowly due to its low natural abundance (0.037%) and small gyromagnetic ratio (-5.774×10^7 MHz T^{-1}) which leads to inherently low sensitivity. In particular, these two factors result in a sensitivity reduction of ∼15 when compared to ^{13}C.[22] In addition, ^{17}O is a quadrupolar nucleus ($I = 5/2$, $Q = -2.558$ fm^2) and the spectra exhibit a significant broadening due to the interaction between the quadrupole moment and the asymmetric electric field gradient in the chemical environments in proteins and nucleic acids.[23] Despite these technical difficulties, ^{17}O is an appealing species to study, since, like nitrogen, it is directly involved in hydrogen bonds, and therefore the chemical shifts are exquisitely sensitive to the chemical environment.[24−26] Furthermore, also like nitrogen, it possesses a large chemical shift range (∼1000 ppm), and in addition an interesting quadrupolar interaction.[27,28] It is therefore important to develop the spectroscopic techniques that allow observation of ^{17}O with high sensitivity.

In the past, modest sensitivity gains for studying ^{17}O NMR were achieved by using isotopic enrichment and applying population transfer techniques.[29,30] It is also possible to remove the second-order quadrupolar interaction in order to obtain simplified isotropic spectra. This requires advanced techniques including special instrumentation, for example, double rotation (DOR) and dynamic-angle spinning (DAS),[31,32] or special spectroscopic techniques such as multiple-quantum magic angle spinning (MQMAS)[33] and satellite-transition magic angle spinning (STMAS).[34] However, when the quadrupole coupling is large (>5 MHz), as is often found for oxygen environments in proteins and nucleic acids, the excitation efficiency of these approaches drops dramatically; in the case of MQMAS spectra, to about ∼5%.[35,36] Thus, although there are a number of exciting MQMAS studies of ^{17}O labeled biological samples, the experimental results are clearly limited by signal-to-noise, hence requiring long acquisition times.[37−46]

Dynamic nuclear polarization (DNP) has been shown to provide immense gains in NMR sensitivity.[47−50] This is accomplished by transferring the large electron spin polarization of unpaired electrons to nuclei via microwave irradiation of the electron−nuclear transitions. For efficient DNP, samples are cooled to cryogenic temperatures (<110 K) where increased electron and nuclear spin−lattice relaxation times (T_{1I}) can assist in a more efficient electron−nuclear spin transfer mechanism. For several compelling reasons including reduced ^{1}H spin−lattice relaxation, improved sensitivity from

Received: August 22, 2013
Revised: November 6, 2013
Published: November 6, 2013

employing cross polarization, and a large database of nitroxide radicals, optimal for ^{1}H cross effect, ^{1}H is often the nucleus of choice for polarization at cryogenic temperatures using a biradical polarizing agent such as TOTAPOL,[51] or other TEMPO biradical variants.[52−56] Subsequent to polarization of ^{1}H, a cross-polarization step is used to observe other low-gamma nuclei (e.g., ^{13}C, ^{15}N, etc.).[47,49,57−61] This method (i.e., indirect polarization, $e^{-} \rightarrow {}^{1}H \rightarrow X$, where X is an NMR active nucleus, such as ^{13}C, ^{15}N, ^{17}O, ^{31}P, etc.) has been successfully applied to membrane proteins, peptides, amyloid fibrils, pharmaceuticals, and surfaces, resulting in an enhancement of NMR signal intensity (ε) between 30- and 180-fold.[9,47,49,57,58,62−76] Many of these studies focused on I = 1/2 nuclei (e.g.,^{13}C, ^{31}P, ^{29}Si, etc.) and reports regarding quadrupolar nuclei have been scarce.[77−81] An alternative to indirect polarization is polarizing an NMR active nucleus (X) directly from an electron spin source, $e^{-} \rightarrow X$ (i.e., direct polarization).[62,77,82−87] This approach is of interest for many chemical systems that cross-polarize by high-γ nuclei (e.g., ^{1}H or ^{19}F) poorly, found within chemical environments where high-γ nuclei are absent or may be of assistance in spectral editing between protonated and non-protonated chemical environments.

Recently, we illustrated the extension of this approach to ^{17}O using indirect polarization via ^{1}H DNP.[78] During that study, we determined that the optimized radical for ^{1}H (i.e., nitroxide-based biradical) performed poorly when polarizing ^{17}O directly.[88,89] Similar observations were observed with the biradical bTbk when studying ^{17}O DNP in two synthetic minerals, periclase (MgO, cubic-$Fm3m$) and brucite ($Mg(OH)_2$, trigonal-$P3m1$).[82] Herein, we report an extensive study for efficient direct polarization of ^{17}O using a series of polarizing agents dissolved in a water/glycerol model system. Utilizing enhancements greater than 100, we also show applications of ^{17}O DNP, which are presented in conjunction with quantum chemical calculations—further extending the ability to use DNP to address problems involving low-gamma quadrupolar systems. The reduction in acquisition time for ^{17}O will likely provide a new approach that can be extended to studies in other chemical systems.

2. THEORY

2.1. Polarization Mechanisms for DNP. Since DNP mechanisms involve the transfer of spin polarization from electrons to nuclei, an exogenous polarizing agent is generally added to the medium containing the solute. Polarizing agents typically are persistent organic mono- or biradicals (e.g., trityl (OX063), SA-BDPA, TOTAPOL, etc.), or more recently high-spin metal complexes.[90] In the case of ^{17}O, a theoretical enhancement of over 4800, determined by the ratio of the gyromagnetic ratios (i.e., γ_e/γ_{17O}), is possible.

At high magnetic fields and temperatures close to liquid N_2, there are two dominant mechanisms that mediate electron−nuclear polarization transfer, (1) the cross-effect (CE) and (2) the solid-effect (SE), and both mechanisms require irradiation of the sample with microwaves of appropriate frequency. In the following, we will briefly outline the salient features of each.

The cross-effect is a three-spin process between two electrons and a nuclear spin that are dipolar coupled.[91−96] The difference between the Larmor frequencies of the two electron spins, determined by their g-values and g-anisotropies (ω_{0S_1}, ω_{0S_2}) must approximate the nuclear Larmor frequency (ω_{0I}) for maximum efficiency:

$$\omega_{0I} = |\omega_{0S_1} - \omega_{0S_2}| \tag{1}$$

For this condition to be met, the inhomogeneous breadth (Δ) of the radical's EPR spectrum is required to be larger than the nuclear Larmor frequency, while the homogeneous component (δ) must be smaller than the nuclear Larmor frequency.

$$\Delta > \omega_{0I} > \delta \tag{2}$$

The solid effect is a two-spin process whereby microwave irradiation is applied at the electron−nuclear zero- or double-quantum frequency.[97]

$$\omega_{mw} = \omega_{0S} \pm \omega_{0I} \tag{3}$$

Due to partial mixing of the nuclear spin states by non-secular electron−nuclear dipolar coupling, these "forbidden" transitions become partially allowed, albeit with a transition moment that is typically 2−3 orders of magnitude smaller than that of the single-quantum EPR transition. Because the zero- and double-quantum transition lead to nuclear enhancements of opposite signs, the homogeneous (δ) and inhomogeneous (Δ) EPR line widths have to be smaller than the Larmor frequency of the nucleus to be polarized in order to avoid overlap and therefore cancellation of positive and negative enhancements:

$$\omega_{0I} > \delta, \Delta \tag{4}$$

Therefore, the SE is the dominant mechanism when polarizing agents with narrow line widths relative to the nuclear Larmor frequency are used.

2.2. NMR Parameters. Since ^{17}O is a quadrupolar nucleus, a coupling between the inherent quadrupole moment and the electric field gradient generated by its surroundings results in a quadrupolar interaction. This coupling will manifest in the observed spectrum and be accompanied by a characteristic shape based on the local symmetry at the ^{17}O site. In solids such as the case for ^{17}O, vide infra, the magnetic field (Zeeman field, B_o) is significantly larger than the quadrupolar interaction. This condition allows us to treat the interaction as a perturbation on B_o, where only the first- and second-order quadrupole interactions are of concern. Hence, the spectra in solids of half-integer quadrupolar nuclei are governed by the quadrupole Hamiltonian

$$\hat{H}_Q = \sum_k \mathbf{I}_k \mathbf{Q}_k \mathbf{I}_k \tag{5}$$

Here $\mathbf{I}_k$ is the nuclear spin operator, the quadrupole coupling tensor $\mathbf{Q}_k$ may be expressed in terms of the electric field gradient tensor $\mathbf{V}_k$ at the kth nuclear site

$$\mathbf{Q}_k = \frac{eQ_k}{2I_k(2I_k - 1)\hbar}\mathbf{V}_k \tag{6}$$

where $\mathbf{V}$ is the electric field gradient at the quadrupolar nucleus, e is the electric charge, $\hbar$ is defined as usual, and Q_k is the quadrupole moment. Taking $V_{k,zz} = eq_k$, we obtain an expression for the first-order frequency

$$\omega_{Qk}^{(1)} = \frac{3e^2 q_k Q_k}{4I_k(2I_k - 1)\hbar} \tag{7}$$

dx.doi.org/10.1021/jp408440z | J. Phys. Chem. B 2013, 117, 14894−14906

The asymmetry is conventionally defined as $\eta_k = (V_{k,xx} - V_{k,yy})/V_{k,zz}$ and leads to the form for the Hamiltonian in the principal axis system where **V** is diagonal with components $|V_{zz}| \geq |V_{yy}| \geq |V_{xx}|$.

$$\hat{H}_{Qk} = \omega_{Qk}\left\{\left(I_{kz}^2 - \frac{1}{3}\mathbf{I}_k^2\right) + \frac{\eta}{3}(I_{kx}^2 - I_{ky}^2)\right\} \quad (8)$$

Although the central transition ($m_I = -1/2 \leftrightarrow +1/2$) is not affected by the first-order quadrupole interaction ($\omega_{Qk}^{(1)}$), its line shape is influenced by a second-order interaction ($\omega_{Qk}^{(2)}$) that scales quadratically with the magnitude of the first-order interaction and inversely with the nuclear Zeeman frequency (ω_{0I}):[97−99] $\omega_{Qk}^{(2)} = (\omega_{Qk}^{(1)})^2/\omega_{0I}$

The nuclear quadrupole interaction is described by a coupling constant, C_Q, $C_{Qk} = (eQV_{zzk}/h)$ that typically ranges between 0 and 12 MHz for ^{17}O and an asymmetry parameter, η, which can assume values between 0 and 1.[28,100−102] A more comprehensive explanation of the quadrupolar interaction for solids can be found elsewhere.[98,103−105]

The chemical shift anisotropy can also influence the appearance of the spectrum, especially under non-spinning conditions and at higher magnetic fields for powdered samples. Although its magnitude is negligible relative to the quadrupole broadening at 5 T for the ^{17}O environments studied here, these parameters should be considered when analyzing higher field spectra.

3. MATERIALS AND METHODS

3.1. Sample Preparation. Samples were prepared using mixtures of d_8-glycerol (60 vol %), D_2O (30 vol %), and H_2O (10 vol %). The H_2O was labeled with oxygen-17 ($H_2{}^{17}O$ − 35%) and was purchased from Cambridge Isotope Laboratories (Andover, MA). Each sample contained 40 mM electron spins homogeneously dispersed at 298 K. The liquid samples were packed into 4 mm o.d. sapphire rotors using between 40 and 60 μL of sample. Samples were prepared with radical concentrations of 20 mM in the case of TOTAPOL and 40 mM trityl (OX063) and SA-BDPA, respectively. Additionally, an equimolar mixture (i.e., 20 mM trityl and 20 mM SA-BDPA) was prepared. For the experiments shown in section 4.5, 40 mM trityl was dissolved together with ^{13}C-^{17}O-urea[106] (~20% ^{17}O) or ^{17}O-phenol (~30% ^{17}O) purchased from Cambridge Isotope Laboratories (Andover, MA) with a concentration of 2.0 and 0.65 M, respectively, in a mixture of d_8-glycerol/D_2O/H_2O (60/30/10 vol %), where H_2O was used in natural abundance (0.037%). A third sample containing 40 mM trityl was prepared following the protocol at the beginning of the section to allow for $H_2{}^{17}O$ NMR analysis. Field profiles were acquired using a mixture of 60/40 (v/v) d_8-glycerol/$H_2{}^{17}O$ (35% - ^{17}O−H_2O) and 40 mM electrons. Please note the ^{17}O background due to natural abundance H_2O (for urea and phenol samples) or hardware (i.e., sapphire-rotor and/or stator materials) can be neglected in comparison to the signals arising from the isotopically enriched analytes for this study, although care should be considered when dealing with alternative materials (e.g., Macor, Al_2O_3, ZrO_2), during MAS at higher magnetic fields and/or low ^{17}O enrichments.

3.2. Dynamic Nuclear Polarization Nuclear Magnetic Resonance. Dynamic nuclear polarization NMR experiments were performed using a home-built spectrometer equipped with a 5 T (^{1}H, 212 MHz) wide bore magnet (courtesy of Dr. D. J. Ruben, FBML, MIT) and a 140 GHz gyrotron with ≤15 W of microwave output. ^{17}O spectra were recorded using a home-built cryogenic double resonance (^{1}H and ^{17}O) DNP NMR probe equipped with a 4 mm Kel-F stator (Revolution NMR, Fort Collins, CO). Microwaves were guided to the DNP probe via a circular corrugated, overmoded waveguide to reduce mode conversion and ohmic losses.[107] At the probe entrance, the waveguide tapers to a fundamental mode, from which microwaves are launched toward the sample.[108,109] Experimental temperatures for all data were maintained below 88 K. Direct ^{17}O polarization experiments were acquired with continuous microwave irradiation, while applying a Hahn-echo sequence on ^{17}O ($\omega_1/2\pi$ = 180 kHz, solid (85 K)) using CW or TPPM^4 proton decoupling ($\omega_1/2\pi$ > 71 kHz). Recycle delays were determined via a saturation recovery sequence which accomplishes saturation using the phase cycling scheme described by Daviso et al.[110] Polarization buildup (T_B) and spin−lattice relaxation (T_{1I}) times between 4.0 and 6.0 s were measured; recycle delays were chosen as $T_B/T_{1I} \times 1.3$.[111] Directly polarized ^{17}O detected DNP field profiles were performed by sweeping the main NMR field using a superconducting sweep coil (±0.1 T) between 4.961 and 4.996 T (211.7 and 212.3 MHz, ^{1}H nuclear Larmor frequency). All spectra were referenced with neat water (15% - $H_2{}^{17}O$) to 0 ppm at 298 K. Simulations of ^{17}O NMR central transition line shapes were performed using SPINEVOLUTION[112] and WSOLIDS.[113] The SPINEVOLUTION software package was used to fit the ^{17}O central-transition line shape by adjusting the C_Q, η, and δ_{iso}. Input files are available within the software package and were adjusted to incorporate the experimental conditions used during acquisition, and varying the apodization. WSOLIDS was also used to simulate the ^{17}O central transition line shape for the non-spinning data to assist in evaluating the experimental uncertainty. Quadrupolar parameters from GIPAW calculations were simulated without further modification within WSOLIDS. To confirm even excitation for these rather broad ^{17}O spectra (i.e., ~100 kHz), on-signals were further investigated using a solid (quadrupolar) echo[114] as well as employing the frequency-stepped[115] or variable offset cumulative spectra (VOCS)[116] method.

3.3. Quantum Chemical Calculations. Electric field gradient and chemical shielding calculations for crystalline ice,[117] urea,[118] and phenol[119] were performed using a gauge-including projector-augmented wave (GIPAW) density functional theoretical method implemented within CASTEP.[120] The Perdew−Burke−Ernzerhof (PBE) functionals are used in the generalized gradient approximation (GGA) for the exchange-correlation energy[121,122] and ultrasoft pseudopotentials.[123] All calculations were performed using the fine accuracy basis set and a maximum plane-wave energy of 550 eV in order to calculate both chemical shieldings and electric field gradients.[124,125] The Monkhorst−Pack grid had a maximum density of up to 4 × 4 × 4 k points. All calculated chemical shieldings ($\sigma_{cal.}$) were referenced with respect to (σ_{ref}) 255.0 ppm (Tables S1−S3, Supporting Information) using ^{1}H optimized (within CASTEP) crystal structures.[126]

4. RESULTS AND DISCUSSION

4.1. Polarizing Agents. Three polarizing agents were studied for direct detection of ^{17}O, incorporated in a water/glycerol glass-forming cryoprotectant. These water-soluble radicals (Figure 1) include TOTAPOL,[51] SA-BDPA,[127] and the OX063 version of trityl.[128]

dx.doi.org/10.1021/jp408440z | J. Phys. Chem. B 2013, 117, 14894−14906

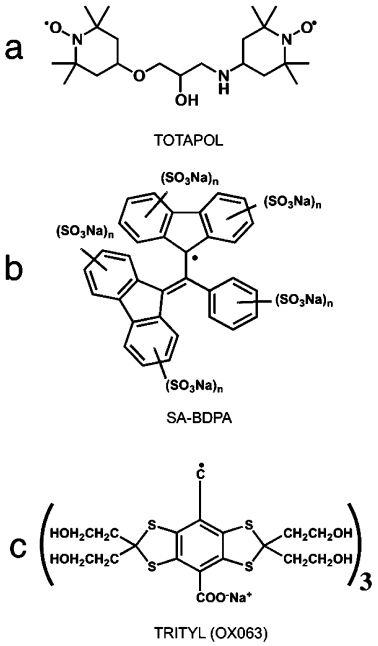

Figure 1. Molecular structures for (a) TOTAPOL (biradical), (b) SA-BDPA (monoradical), and (c) trityl-OX063 (monoradical) polarizing agents capable of directly polarizing ^{17}O.

The EPR spectrum of the biradical TOTAPOL introduced by Song et al.[51] largely resembles that of the monomeric TEMPO radical precursor and displays a large *g*-anisotropy, resulting in an asymmetric inhomogeneous spectrum with $\Delta \geq$ 600 MHz at 5 T. SA-BDPA and trityl are both monomeric radicals and exhibit narrow, approximately symmetric EPR spectra with inhomogeneous line widths on the order of 28 and 50 MHz, respectively.[127] We have shown that cross-effect DNP of ^{1}H followed by cross-polarization is the optimal approach thus far in studying a variety of biological systems.[9,59,63,64,66,67,78,94,129,130]

With the advent of higher powered microwave devices and the use of paramagnetic metal centers, the solid effect is also of interest, providing significant enhancements can be obtained at elevated fields.[131] To better understand these radicals and the dominant DNP mechanism for direct ^{17}O polarization, we studied ^{17}O detected field profiles and enhancements.

4.2. Field Profiles. Since direct polarization of ^{17}O is in its nascence, we must carefully study both the radical and field profile in order to determine the dominant DNP mechanism for this low-γ nucleus with a nuclear Larmor frequency approximately 1/7th that of ^{1}H (~28.8 MHz at 5.0 T). Field profiles for each polarizing agent are shown in Figure 2. The DNP field profile obtained using TOTAPOL closely resembles the profile when ^{1}Hs are polarized under similar conditions, exhibiting a slight upfield shift of the DNP maximum (4.9789 T).[51] It is important to note that the maximum negative enhancement (4.9691 T) using the biradical TOTAPOL is actually ~20% higher than the maximum positive enhancement. The negative lobe of the field profile is also narrower (i.e., sharper) for ^{17}O than when studying the indirect field profile (i.e., ^{1}H).[78] Similar effects have been seen for directly detected DNP of low-γ nuclei and the polarizing agent TOTAPOL[77,85] and bTbk,[82] as a more favorable enhancement is found at the field of maximum negative enhancement. We would like to point out that significant quadrupolar interaction leads to enhanced nuclear relaxation and a broad NMR spectrum that may affect the CE performance. Furthermore, the experiments in this study are performed on static samples, since quadrupolar effects are too strong to be efficiently averaged by magic angle spinning (see Supporting Information Figures S5 and S6), whereas above-mentioned experiments on low-γ nuclei have been carried out under MAS conditions.

In contrast to TOTAPOL, SA-BDPA has a narrow ^{17}O field profile with nearly symmetric positive and negative maxima at 4.9833 and 4.9806 T, respectively. The decreased breadth of the profile is directly related to the significantly narrower EPR spectrum of SA-BDPA with respect to TOTAPOL. This narrow width occurs due to a small inhomogeneity caused by hyperfine coupling to intramolecular ^{1}H, while the *g*-tensor anisotropy is vanishing.[127] Furthermore, the isolated positive

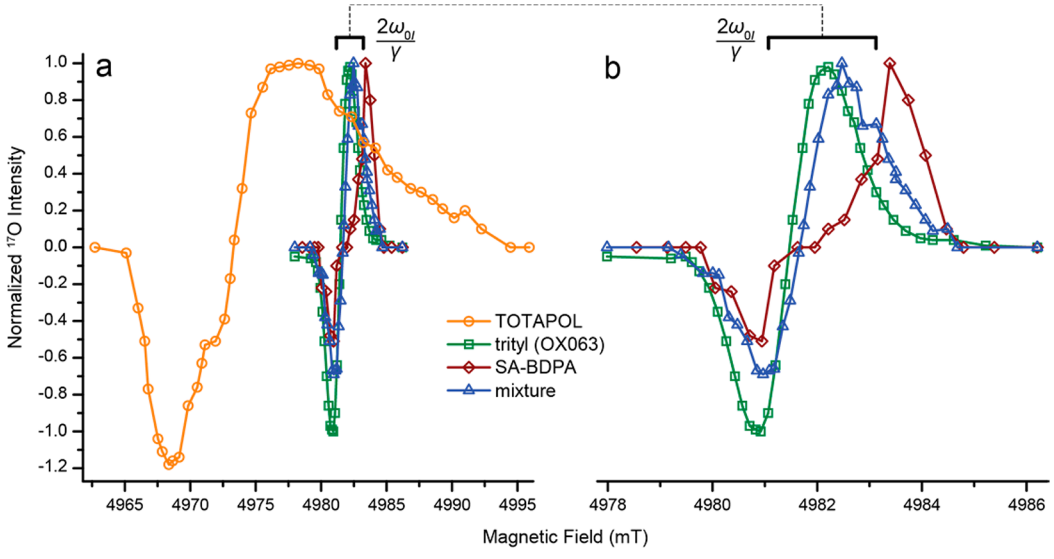

Figure 2. (a) ^{17}O detected field profiles for (circles, orange) TOTAPOL (96 scans/point), (squares, green) trityl (8 scans/point), (diamonds, red) SA-BDPA (384 scans/point), and (triangles, blue) SA-BDPA-trityl mixture (16 scans/point). (b) Expanded region for the three narrow-line radical field profiles. The sample composition for field profiles was 60/40 (v/v) d_8-glycerol/$H_2{}^{17}O$ (35%-^{17}O–H_2O) with 40 mM electrons.

dx.doi.org/10.1021/jp408440z | J. Phys. Chem. B 2013, 117, 14894–14906

and negative enhancement peaks are separated by 68 ± 7 MHz in the EPR domain with a flat plateau in the center, indicative of a dominant solid-effect polarization mechanism. However, we note that this separation is significantly larger than the expected separation by $2\omega_{0I}$ = 57.4 MHz. The reason for that discrepancy is unclear. It might be caused in part or whole by the relatively low signal enhancement and therefore large error in the extrema of the field profile. At the same time, the quadrupolar properties might lead to a slightly different SE matching condition, vide infra. In any case, the large separation clearly rules out CE as the DNP mechanism. Trityl exhibits a similar narrow field profile, with symmetric positive (4.9820 T) and negative (4.9808 T) enhancement lobes. The trityl field profile is similar to those of other low-γ nuclei studied (^{2}H and ^{13}C).[77,86] The large ratio of the inhomogeneous breadth, $\Delta \approx$ 50 MHz, of the near symmetric EPR spectrum of trityl and the nuclear Larmor frequency, ω_{0I} = 29 MHz (at 5 T), leads to a highly symmetric and unstructured field profile dominated by the CE (see eq 2). This is in contrast to other studies of ^{13}C DNP using trityl, where $\Delta \approx \omega_{0I}$ and SE played an equally important role as the DNP mechanism besides CE.[86]

The field position of the negative enhancement from trityl and/or SA-BDPA is useful because a slight adjustment in field from the maximum of TOTAPOL for ^{1}H (4.9798 T) enables one to reach the position for maximum negative DNP enhancement of low-γ nuclei (e.g., ^{2}H, ^{13}C, and ^{17}O) at 4.9808 T. This permits the direct polarization of ^{17}O or other low-γ nuclei using trityl and their indirect polarization via ^{1}H using TOTAPOL without further adjustment of the external magnetic field.

4.3. Enhancements. To evaluate the efficiency of polarization transfer and enhancements, a series of samples were studied, each using a concentration of 40 mM electron spins of the three polarizing agents. Saturation recovery experiments were performed to determine the effective T_B for direct oxygen detection using SA-BDPA, TOTAPOL, and trityl. Common issues surrounding direct detection for many spins other than ^{1}H are the long buildup and relaxation times, and the drastic increases in these parameters associated with a decrease in temperature. The combination of the presence of the paramagnetic species in solution, the system being in a disordered state, and oxygen bearing quadrupolar properties (i.e., quadrupolar relaxation) promotes efficient longitudinal relaxation. This enables the use of reasonable recycle delays, comparable to those applied for ^{1}H. DNP buildup times were measured for each sample; T_B of 5.2, 4.2, and 5.0 s were determined for SA-BDPA, TOTAPOL, and trityl, respectively (Table 1).

By maintaining identical sample conditions for SA-BDPA, TOTAPOL, and trityl samples and adjusting only the polarizing agent, the absolute enhancements were determined to be ε = 3, 7, and 115, respectively (Table 1, Figure 3). The gain in sensitivity is further increased due to the larger Boltzmann factor at T = 85 K, adding gains of approximately 3.5 ($\varepsilon^{\dagger}$ = 10, 25, and 400, respectively).

The I = 5/2 ^{17}O nucleus poses several differences compared to the typically I = 1/2 system (e.g., ^{1}H, ^{13}C, ^{29}Si, ^{31}P, etc.) such as six energy levels (i.e., ± 1/2, ± 3/2, and ±5/2) and multiple allowed transitions. Furthermore, quadrupolar nuclei in the solid state experience a significant dispersion of resonance frequencies unless they are situated in a cubic (isotropic) environment. For covalently bound ^{17}O, this dispersion covers a range of up to 9 MHz independent of the external magnetic field strength. Therefore, the matching conditions for the CE and SE in principle are altered to represent the effective Larmor frequency rather than just the Zeeman frequency. This translates the dispersion in the nuclear frequency domain into a dispersion in the matching condition between nuclear spin frequencies and the required irradiation frequency of electron spins, as well as the shape of the DNP field profiles. However, the central transition ($m_I = -1/2 \rightarrow +1/2$) is an exception to this dispersion. The residual second-order broadening of ~90 kHz (for ^{17}O in a frozen glass environment at 5 T) can be neglected with respect to the magnitude of the EPR line widths of at least several tens of MHz, and naively, one tends to simply utilize the matching conditions eqs 1 and 3.

Nevertheless, several reasons argue against this simplification. The eigenframes of all nuclear m_I states are significantly tilted with respect to the external magnetic field axis absent in the fortuitous case of colinearity between the EFG tensor and the external magnetic field (i.e., the external magnetic field vector is oriented along one of the canonical orientations of the EFG).

Table 1. ^{17}O Enhancements and Buildup Times for Direct Polarization of Oxygen in a 60/30/10 (v/v) d_8-Glycerol/D_2O/$H_2{}^{17}O$ (35%-^{17}O−H_2O) with 40 mM Electrons and a Sample Temperature of 85 K[a]

radical	DNP mechanism	ε	T_B[d] (s)	T_{1S} (ms)
SA-BDPA	SE	3 ± 0.6	5.2	28.9[86]
TOTAPOL	CE	7 (−8)[b] ± 1	4.2	~0.3[132]
trityl (OX063)	CE	115 ± 11	5.0	1.4[86]
mixture	CE	40 ± 6	5.7	1.4/3.6[c,86]

[a]All enhancements were acquired at the field position of maximum positive value with and without microwaves. [b]^{17}O DNP enhancement for the biradical; TOTAPOL is non-symmetric; the value in parentheses is the enhancement determined at the maximum negative enhancement point with and without microwaves. [c]Values for trityl and SA-BDPA components, respectively. [d]Nuclear spin−lattice relaxation times (T_{1I}) were measured independently (microwaves off) and found to be within experimental error to the DNP buildup relaxation times (T_B).

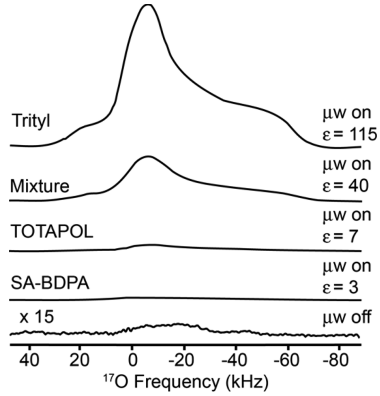

Figure 3. Direct polarization of ^{17}O in 60/30/10 (v/v) d_8-glycerol/D_2O/$H_2{}^{17}O$ using 35% labeled ^{17}O water and 40 mM electrons, using 9 W of microwave power. Radicals are arranged from highest enhancement to lowest, with trityl (16 scans, ~2 min), mixture (64 scans, ~8 min), TOTAPOL (608 scans, ~60 min), and SA-BDPA (1664 scans and ~180 min), and the microwaves off ×15 (6646 scans, ~12 h) spectrum from the trityl sample. NB: Enhancements and uncertainties in Table 1 were determined by acquiring an on/off signal on the same sample; the bottom trace in the figure is the off spectrum for the trityl radical and is included here for reference purposes.

dx.doi.org/10.1021/jp408440z | J. Phys. Chem. B 2013, 117, 14894−14906

This tilting leads to significant mixing of the nuclear states. The states are coupled by the non-secular quadrupole interaction components, which are on the order of a few MHz. These couplings are typically much larger than those leading to the electron−nuclear double- and zero-quantum coherences invoked during SE DNP and will therefore affect the state mixing which is a prerequisite for SE. Additional coherences are introduced, which couple the central transition states (i.e., $|m_I| = 1/2$) to those with $|m_I| > 1/2$. Although these transitions are generally off-resonant under SE matching, fast oscillations to these states might compete with the SE transfer and allow for additional nuclear relaxation pathways (vide infra). For the CE, the situation is slightly more complicated because two types of coherences are involved: electron−electron and electron−nuclear dipole coupling between one of the electron spins and the nuclear spin polarized. The former typically is larger than the quadrupole interaction if biradicals are used as polarizing agents (e.g., ∼25 MHz for TOTAPOL), whereas it approaches the coupling if intermolecular couplings are involved in the case of monoradicals. The electron−nuclear dipole coupling again is expected to be smaller than the nuclear quadrupolar interaction; however, it might also be of similar order, since the polarization pathway is less clear than in the SE case. Furthermore, the direct impact of electron−electron and electron−nuclear coupling is not completely understood for the CE; therefore, effects that quadrupolar nuclei impose on the CE efficiency are not clear.

Besides the effect of the quadrupole coupling, non-coherent relaxation processes will affect the DNP transfer. The nuclear quadrupolar interaction leads to very efficient spin−lattice relaxation, competing directly with buildup of enhanced polarization by DNP. Corzilius et al.[133] have introduced a DNP equilibrium constant K_{DNP} which is calculated from the enhancement factor and takes into account the DNP rate constant k_{DNP} and the nuclear spin−lattice relaxation time constant T_{1I}:

$$K_{DNP} = k_{DNP}T_{1I} = \frac{(\varepsilon_\infty - 1)}{\left(\frac{P_S^\infty}{P_{I,eq}} - \varepsilon_\infty\right)} \approx \frac{(\varepsilon_\infty - 1)}{(\varepsilon_{max} - \varepsilon_\infty)} \approx \frac{\varepsilon_\infty}{\varepsilon_{max}}$$
$$\text{for} \quad 1 \ll \varepsilon_\infty \ll \varepsilon_{max} \tag{9}$$

P_S^∞ and $P_{I,eq}$ describe the residual electron polarization after infinite polarization time and the nuclear polarization in thermal equilibrium, respectively; ε_{max} is the thermodynamically maximum achievable enhancement: $\varepsilon_{max} = \gamma_S/\gamma_I$; and ε_∞ is the enhancement (ε) after infinite polarization time. For the first approximation in eq 9, it is assumed that the effective electron polarization is not depleted during DNP transfer, which is the case when electron longitudinal relaxation is fast. With this equation, we can estimate the effect of fast quadrupolar relaxation on the experimentally observed enhancement. Under this assumption, we find that $K_{DNP} \ll 1$, so that ε_{max} must be much larger than ε_∞. Therefore, we can finally replace $\varepsilon_{max} - \varepsilon_\infty$ with ε_{max} and $\varepsilon_\infty - 1$ with ε_∞. In this case, the observed enhancement scales linearly with T_{1I}. We note that T_{1I} only accounts for spin−lattice relaxation including paramagnetic relaxation enhancement (PRE); DNP effects that shorten the experimentally observed time constant have to be excluded. For the SE, this is trivial, since DNP is only active when the electron−nuclear spin system is irradiated with the appropriate microwave frequency. In this case, the DNP buildup rate constant and the spin−lattice relaxation rate constant additively form the observed overall buildup rate constant $1/T_B$:

$$\frac{1}{T_B} = k_{DNP} + \frac{1}{T_{1I}} \tag{10}$$

The CE, however, is always active, because the driving coherences are introduced by the electron−electron coupling, which cannot be switched off; however, in thermal equilibrium, no net polarization transfer occurs because the rates for positive and negative enhancement of nuclear polarization are equal. In this case, net polarization transfer is achieved by disturbing the thermal equilibrium polarization of one of the electron spins by microwave irradiation induced saturation and the resulting change in one of the DNP rate constants. Therefore, a disentanglement of rate constants according to eq 10 is not possible.

The observed buildup time constants in Table 1 clearly show a rather uniform distribution with an average of 5.0 s and a small maximum deviation of only 0.8 s. This deviation lies well within the error of the experiments, especially given the small absolute signals when small enhancements are encountered. This leads us to the conclusion that all T_B's are limited by short T_{1I}, and that k_{DNP} is rather small in all cases. Despite this theoretically unfavorable situation, trityl allows for a significant enhancement of 115, which results in more than a factor of 13 000 reduction of acquisition time. TOTAPOL, on the other hand, yields only $\varepsilon = 7$. The discrepancy between trityl and TOTAPOL is explained by the dramatically different EPR line shapes. While trityl has a Gaussian-like line shape with $\Delta = 50$ MHz, the overall breadth of the TOTAPOL powder line shape due to the g-anisotropy is ∼600 MHz at 5 T. Therefore, the trityl spectrum concentrates the electrons in a more narrow spectral region for efficient ^{17}O CE matching with $\omega_{0^{17}O} \approx 29$ MHz. This demonstrates the potential of radicals with a narrow EPR line as effective polarizing agents for CE DNP of low-γ nuclei. We reported similar observations when directly polarizing ^2H.[77]

SA-BDPA yields a rather small enhancement $\varepsilon = 3$. We attribute this to the fact that the SE is active in this case, and also affected by a large quadrupole coupling. Even though a reduction of T_B with respect to T_{1I} is expected for the SE, we have observed $T_B \approx T_{1I}$ within the experimental error for all samples, including SA-BDPA. According to eq 10, this leads us to conclude that $k_{DNP} \ll 1/T_{1I}$ and is in line with the very small observed enhancement. Another potential problem is the depletion of the electron spin polarization by off-resonant saturation of the EPR resonance. The combination of extremely long $T_{1S} = 29$ ms and small resonance offset of $\omega_{0I} = 29$ MHz is supposed to significantly reduce the electron spin polarization available for transfer to nuclear spins by off-resonance irradiation of the EPR transition.[131]

It would seem that nuclear relaxation is a significant factor in obtaining effective DNP gains as both ^2H ($\omega_{0I} = 32.5$ MHz, $I = 1$) and ^{17}O ($\omega_{0I} = 28.7$ MHz, $I = 5/2$) are quadrupolar and their respective nuclear Larmor frequencies are similar. ^2H detection on identical samples exhibited an enhancement >500 with a T_B of 70 s, whereas ^{17}O direct detection was $\varepsilon = 115$ and T_B of 5 s. If ^{17}O T_{1I} relaxation rates could be reduced, we surmise that the enhancements would increase.

Further enhancements could be gained from magic-angle spinning at a moderate frequency (Figure S6, Supporting Information). Rotating the sample has several effects that lead to improved DNP efficiency: including a reduction of certain

dx.doi.org/10.1021/jp408440z | J. Phys. Chem. B 2013, 117, 14894−14906

anisotropies and an increase in the efficiency of polarizing by allowing the microwaves to average over the full surface of the rotor. Our group and others have noted gains in enhancement when studying systems under MAS conditions.[59] We will report on non-spinning and MAS experiments at higher fields in a future publication.

4.4. Mixture. In theory, the CE mechanism is most efficient when two narrow EPR lines are separated by the nuclear Larmor frequency while an appropriate coupling allows for transfer of polarization between the two lines.[95,96] The concept has first been demonstrated by Hu et al. by mixing the narrow-line radical trityl with the nitroxide radical TEMPO.[91] Irradiation on resonance with the center of the trityl EPR transition resulted in a 4-fold increase of enhancement compared to the use of TEMPO as a polarizing agent alone. Therefore, a mixture of SA-BDPA and trityl OX063 might allow for cross effect, where the SA-BDPA resonance is irradiated with microwaves and polarization is transferred to a dipolar coupled nucleus during an electron−electron cross-relaxation flip-flop between SA-BDPA and trityl; this approach was illustrated to work extremely well in the case of direct ^{13}C DNP NMR.[86] In an attempt to improve the enhancement of SA-BDPA, a mixture of 20 mM SA-BDPA and 20 mM trityl in a water/glycerol glass was acquired. The field profile is shown in Figure 2b; the profile indicates a cross-effect mechanism with a broadened inhomogeneous line width and a positive maximum (4.982 T). The overall enhancement improved to 40 from 3 (Figure 3). Note that the maximum positive enhancement position coincides with the EPR resonance field of SA-BDPA together with the asymmetry between the positive and negative maxima indicates that the CE is active between SA-BDPA and trityl. The asymmetry was reported by Hu et al.[91] and is caused in part by different longitudinal relaxation properties of the radicals involved. In particular, SA-BDPA has a T_{1S} that is significantly longer than that of trityl.[127] Subsequently, irradiation at the EPR resonance of SA-BDPA leads to a very effective spin saturation, and polarization can be efficiently replenished by fast-relaxing trityl in a cross-relaxation process. Irradiation of the trityl spin on the other hand would be less efficient due to faster T_{1I} relaxation, while cross-relaxation would saturate the slowly relaxing SA-BDPA, effectively quenching the CE.

4.5. Structurally Relevant Oxygen Environments. The ability to polarize ^{17}O directly and indirectly (through ^{1}H) has enabled this challenging nucleus to be used within a variety of 1D and 2D experiments as a probe for local oxygen environments, which vary within organics, proteins, sugars, surfaces, and oxides. Three common functional groups providing a unique oxygen environment can be envisioned for aiding in structural elucidation of various chemical systems. First, water (H_2O) plays an important role in hydrogen bonding, transport, and surface chemistry. Second, carbonyl (C═O), a double-bonded oxygen, is integral to protein structure, folding, and function. Third, a hydroxyl (—OH) moiety is often associated with hydration−dehydration reactions, hydrogen bonding, and layered hydroxides. To illustrate the widespread ability of DNP on oxygen environments, ^{17}O spectra of three small molecules are discussed below using direct polarization ^{17}O DNP NMR, room temperature NMR experiments on the crystalline solid (without DNP), and quantum chemical calculations for crystalline water, urea, and phenol using GIPAW.

DNP of water environments was recently illustrated using the indirect polarization method via DNP of ^{1}H followed by cross-polarization.[78] As water is frozen, a variety of arrangements can occur (e.g., Ice-Ih, Ice-XI, etc.) depending on temperature, isotopic content (^{1}H:^{2}H), freezing rate, and pressure.[134] The frozen solution studied is comprised of a cryoprotecting solvent in an amorphous state, whereby crystal packing is inhibited. Nevertheless, with the significant gains offered by DNP, the quadrupolar NMR parameters can still be determined. A moderate quadrupole coupling constant of 6.8 MHz in magnitude was obtained by spectral simulation of the central transition. The asymmetry parameter and isotropic chemical shift were 0.95 and 0 ppm, respectively, and agree well with literature studies of frozen water.[135,136] An ordered ice crystal structure,[117] which apparently occurs at cryogenic temperatures, was calculated using GIPAW in order to evaluate the calculated oxygen NMR properties, crystal structure, and DNP NMR experimental data. The two crystallographic oxygen sites contained quadrupolar coupling constants of −6.632 and −7.034 MHz with asymmetry parameters of 0.91 and 0.88. The averages of these two sites agree well with the experimentally determined parameters above (Figure 4 and Table 2).

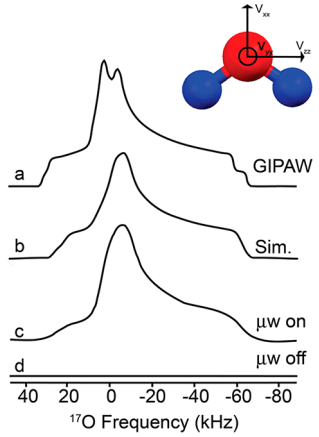

Figure 4. ^{17}O DNP NMR spectrum of water using direct polarization from trityl. (a) Simulation using GIPAW calculated parameters for crystal structure, (b) simulation of quadrupolar line shape, (c) experiment on-signal for amorphous sample (64 scans, ∼7 min), and (d) experiment off-signal (6646 scans, ∼12 h). Sample conditions: 60/30/10 (v/v) d_8-glycerol/D_2O/$H_2{}^{17}O$ using 35% labeled ^{17}O water and 40 mM trityl.

Practically all high-field DNP based studies on biological proteins involve a cryoprotecting matrix with approximately 40% water. This potentially creates a challenge when studying oxygen environments within solutes that need to be dispersed within water, as the labeled oxygen sites may compete with the high molarity of the natural abundance oxygen in water (i.e., 55 M oxygen). To illustrate both the major boost in sensitivity of DNP on oxygen and to provide evidence that natural abundant background oxygen is not an issue, organic based carbonyl and hydroxyl small molecules were studied using 3−4 mg of ≤30% labeled ^{17}O. The small sample volume and low enrichments are important aspects for validating DNP, as ^{17}O labeling is at present costly and limited concentration within biological solids.[137]

The central transition ^{17}O DNP NMR spectrum of urea, $(NH_2)_2C{=}{}^{17}O$, a representative C═O, is shown in Figure 5 with and without microwave radiation. Determining the exact

dx.doi.org/10.1021/jp408440z | J. Phys. Chem. B 2013, 117, 14894−14906

Table 2. Experimental (DNP and Non-DNP) and Calculated ^{17}O NMR Parameters for Model Oxygen Environments

molecule	C_Q (MHz)	η	δ_{iso} (ppm)	Ω (ppm)	κ
water (DNP)	6.8 (2)	0.95 (5)	0 (150)	n.d.	n.d.
water (exp.)[a]	6.43	0.935	n.d.	n.d.	n.d.
water (exp.)[b]	6.66	0.935	0	n.d.	n.d.
water (GIPAW)[e]	−6.833	0.90	−68.24	35.59	−0.40
urea (DNP)	7.5 (3)	0.5 (2)	150 (150)	n.d.	n.d.
urea (exp.)[c]	7.24	0.92	108	280	−0.857
urea (GIPAW)	7.576	0.96	172.37	262.98	−0.82
phenol (DNP)	8.3 (3)	0.95 (5)	100 (150)	n.d.	n.d.
phenol (exp.)[d]	8.3 (1)	0.95 (5)	80 (5)	n.d.	n.d.
phenol (GIPAW)[e]	−8.686	0.84	81.61	71.12	0.53

[a]Ba et al.[136] [b]Spiess et al.[135] [c]Dong et al.[106] [d]^{17}O MAS NMR data acquired at 17.4 T (see Figure S4, Supporting Information). [e]Where multiple crystallographic oxygen sites existed, the averages of these are presented within the table (please refer to the Supporting Information, Tables S1−S3). Experimental uncertainties are given in parentheses. The Herzfeld−Berger[141] convention is used to describe the chemical shift anisotropy, with the span (Ω) and skew (κ) defined as $\Omega = (\delta_{11} - \delta_{33})$ and $\kappa = 3(\delta_{22} - \delta_{iso})/\Omega$, respectively.

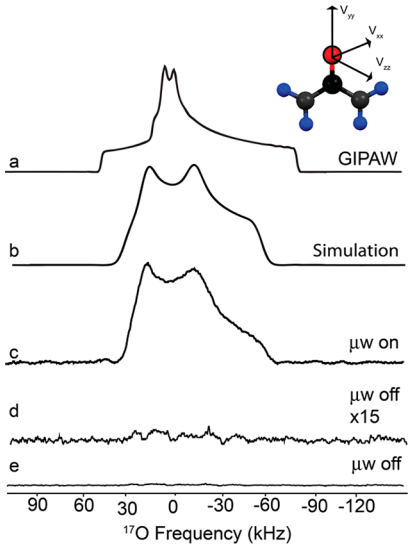

Figure 5. ^{17}O DNP NMR spectrum of ^{17}O labeled urea (4 mg) in 60/30/10 (v/v) d_8-glycerol/D_2O/H_2O and 40 mM trityl using direct polarization. (a) Simulation using GIPAW calculated parameters, (b) simulation of quadrupolar line shape, (c) experiment on-signal (∼8 h), (d) experiment off-signal scaled by 15, and (e) experiment off-signal (∼144 h).

^{17}O DNP enhancement is difficult due to the poor S/N ratio from the collected off spectrum; nonetheless, the enhancement is ≥80. The quadrupolar coupling parameters (C_Q = 7.5 MHz and η = 0.5) and isotropic chemical shift (δ_{iso} = 150 ppm) were obtained by spectral simulation (Figure 5b) of the ^{17}O central transition (Figure 5c). The off spectrum was acquired for 6 days (144 h) under identical conditions with little success, thus limiting our ability to quantify ε. Thus, without DNP, this experiment would have been impossible due to the small gyromagnetic ratio, sample volume, and large quadrupolar coupling.

The quadrupolar coupling determined experimentally by DNP and calculated using GIPAW agree quite well with the experimental (non-DNP) solid-state NMR data acquired on crystalline urea[106] (Table 2). One parameter, however, is poorly represented, which is the asymmetry parameter of the cryoprotected small molecule (Figure 5). We experimentally observed $\eta \sim 0.5$, while, in the crystalline sample, $\eta \sim 1$ due to the C_{2v} point group symmetry of urea which is the same as that for water. Previous studies of crystalline urea by Dong et al.[106] illustrated the importance of incorporating the long-range structure for accurate Gaussian-based calculations in order to calculate the asymmetry parameter properly. With gas-phase based calculations, they illustrated that the asymmetry parameter changes from 0.6 to 0.9 as they constructed the surrounding environment around a single urea molecule, indicating that the hydrogen bonding arrangement is important in determining η. Urea solubilized in the cryoprotectant lacks the local environment of the crystalline phase and hence affects the packing, hydrogen bonding, and effective EFG. Therefore, we attribute this change with the EFG to a "solvent effect" that should be considered when studying small molecules with large chemical shieldings or quadrupolar coupling constants as different asymmetry parameters may be observed.[138,139]

Phenol, a hydroxyl containing aromatic ring, is often associated with tyrosine-like residues and provided ε > 100, as shown in Figure 6. As in the case of urea, the off signal (acquired for 6 days) and the on signal (acquired for ∼18 h) exhibited no interference from the oxygen present in the cryoprotectant (or rotor). The line shape spans over 4500 ppm (>130 kHz) with an associated distribution of sites (disordered, glass-like structure), causing further broadening of the central region (similar to H_2O). The experimental ^{17}O NMR parameters were determined in a fashion similar to that described above with a quadrupolar coupling constant of 8.3 MHz, asymmetry parameter of 0.88, and isotropic chemical shift of 100 ppm. GIPAW calculations and NMR experiments of the crystalline solid (non-DNP) at higher magnetic fields (Table 2, Figure S4, Supporting Information) agree well with experimental parameters as well as other phenolic-like systems studied previously.[100,140]

Three distinct oxygen environments (i.e., water, carbonyl, and hydroxyl) using trityl as a polarizing agent lead to enhancements >80. The ability to fit NMR parameters, in particular quadrupolar couplings, which are in reasonable agreement with experimental data acquired at room temperature illustrates the strength of this method for sensitivity gains. The experimentally determined ^{17}O quadrupolar coupling constants from DNP agree well with those obtained from the room temperature NMR data of the crystalline solids (non-DNP) and are reproduced well by the GIPAW based calculations (Figure S1−S3, Tables S1−S3, Supporting Information). However, care is advised when recording spectra of quadrupolar and/or highly polarizable nuclei at low

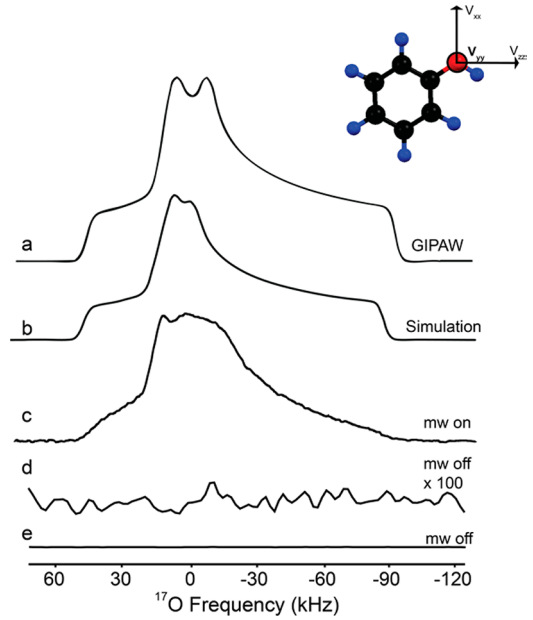

Figure 6. ^{17}O DNP NMR spectrum of ^{17}O labeled phenol (3 mg) in 60/30/10 (v/v) d_8-glycerol/D_2O/H_2O and 40 mM trityl using direct polarization. (a) Simulation using GIPAW calculated parameters, (b) simulation of quadrupolar line shape, (c) experiment on-signal (~18 h), (d) experiment off-signal scaled by 100, and (e) experiment off-signal (~144 h).

temperatures and in a cryoprotecting solvent, as both the asymmetry parameter and chemical shielding parameters (i.e., η, δ_{iso}, Ω, and κ) are known to be highly sensitive to local chemical environments. DNP is an ideal tool for studying microcrystalline environments which will have limited solvent and temperature effects, enabling the potential to combine DNP with NMR crystallography methods[142] for studying difficult NMR nuclei in other chemical systems.

5. CONCLUSION

The direct DNP of ^{17}O has been demonstrated on typical oxygen environments relevant to the study of molecular biology. The array of radicals available is vast; however, the three most prominent, currently used polarizing agents illustrate the ability to polarize ^{17}O directly without the need of protons. This enables a method to study oxygen environments that lack the presence of ^{1}H for CP. Although all radicals discussed provide gains over conventional room temperature NMR, trityl yields the greatest enhancements, while the system offers experimentally convenient relaxation times at cryogenic temperatures. The gains in sensitivity for this spectroscopically difficult quadrupolar nucleus provide significant savings in acquisition time. This provides new opportunities for studying ^{17}O by NMR, enabling extension to multidimensional studies or studies of small sample sizes with isotropic labeling. As DNP moves toward higher magnetic fields and higher frequency spinning, this technique should prove promising in the study of biological, medical, and material applications.

■ ASSOCIATED CONTENT

Supporting Information

GIPAW calculations, high field ^{17}O NMR, MAS DNP NMR, variable field MAS NMR simulations, Tables S1−S3, and Figures S1−S6. This material is available free of charge via the Internet at http://pubs.acs.org.

■ AUTHOR INFORMATION

Corresponding Author

*E-mail: rgg@mit.edu.

Present Addresses

†B.C.: Institute of Physical and Theoretical Chemistry, Institute of Biophysical Chemistry, and Center of Biomolecular Magnetic Resonance (BMRZ), Goethe University Frankfurt, Max-von-Laue-Str. 7, 60438 Frankfurt, Germany.

‡A.A.S.: Department of Chemistry and Applied Biosciences, Laboratory of Physical Chemistry, ETH-Zürich, CH-8093 Zürich, Switzerland.

Notes

The authors declare no competing financial interest.

■ ACKNOWLEDGMENTS

Research reported in this publication was supported by the National Institute of Biomedical Imaging and Bioengineering of the National Institute of Health under award numbers EB-002804, EB-003151, EB-001960, and EB-002026. The authors would like to thank E. Daviso, T.-C. Ong, C. Wilson, A. Thakkar, J. Bryant, R. Lundgren, C. Turner, and D. Ruben for valuable discussions throughout the course of this research, Ms. O. Hayes and Prof. T. Swager for supplying the SA-BDPA radical, and Dr. V. Terskikh (National ultrahigh-field NMR Facility for solids, NRC, Ottawa, Canada) for his assistance with access to the CASTEP software. V.K.M. is grateful to the Natural Sciences and Engineering Research Council of Canada for a postdoctoral fellowship. B.C. acknowledges receipt of a research fellowship from the Deutsche Forschungsgemeinschaft (CO 802/1-1).

■ REFERENCES

(1) Pines, A.; Gibby, M. G.; Waugh, J. S. Proton-Enhanced Nuclear Induction Spectroscopy. Method for High-Resolution NMR of Dilute Spins in Solids. *J. Chem. Phys.* **1972**, *56* (4), 1776−1777.

(2) Andrew, E. R.; Bradbury, A.; Eades, R. G. Nuclear Magnetic Resonance Spectra from a Crystal Rotated at High Speed. *Nature* **1958**, *182*, 1659−1659.

(3) Lowe, I. J. Free Induction Decays of Rotating Solids. *Phys. Rev. Lett.* **1959**, *2* (7), 285−287.

(4) Bennett, A. E.; Rienstra, C. M.; Auger, M.; Lakshmi, K. V.; Griffin, R. G. Heteronuclear Decoupling in Rotating Solids. *J. Chem. Phys.* **1995**, *103* (16), 6951−6958.

(5) Comellas, G.; Lopez, J. J.; Nieuwkoop, A. J.; Lemkau, L. R.; Rienstra, C. M. Straightforward, Effective Calibration of SPINAL-64 Decoupling Results in the Enhancement of Sensitivity and Resolution of Biomolecular Solid-State NMR. *J. Magn. Reson.* **2011**, *209*, 131−135.

(6) Detken, A.; Hardy, E. H.; Ernst, M.; Meier, B. H. Simple And Efficient Decoupling In Magic-Angle Spinning Solid-State NMR: The XiX Scheme. *Chem. Phys. Lett.* **2002**, *356*, 298−304.

(7) Fung, B. M.; Khitrin, A. K.; Ermolaev, K. An Improved Broadband Decoupling Sequence for Liquid Crystals and Solids. *J. Magn. Reson.* **2000**, *142*, 97−101.

(8) Rienstra, C. M.; Tucker-Kellogg, L.; Jaroniec, C. P.; Hohwy, M.; Reif, B.; McMahon, M. T.; Tidor, B.; Lozano-Perez, T.; Griffin, R. G. De novo Determination of Peptide Structure with Solid-State Magic-Angle Spinning NMR Spectroscopy. *Proc. Natl. Acad. Sci. U.S.A.* **2002**, *99* (16), 10260−10265.

(9) Bajaj, V. S.; Mak-Jurkauskas, M. L.; Belenky, M.; Herzfeld, J.; Griffin, R. G. Functional and Shunt States of Bacteriorhodopsin Resolved by 250 GHz Dynamic Nuclear Polarization-Enhanced Solid-

State NMR. *Proc. Natl. Acad. Sci. U.S.A., Early Ed.* **2009**, *106*, 9244−9249.
(10) Cady, S. D.; Schmidt-Rohr, K.; Wang, J.; Soto, C.; DeGrado, W.; Hong, M. Structure of the Amantadine Binding Site of Influenza M2 Proton Channels in Lipid Bilayers. *Nature* **2010**, *463*, 689−692.
(11) Castellani, F.; van Rossum, B.; Diehl, A.; Schubert, M.; Rehbein, K.; Oschkinat, H. Structure of a Protein Determined by Solid-State Magic-Angle-Spinning NMR Spectroscopy. *Nature* **2002**, *420* (6911), 98−102.
(12) Eddy, M. T.; Ong, T.-C.; Clark, L.; Teijido, O.; van der Wel, P. C. A.; Garces, R.; Wagner, G.; Rostovtseva, T.; Griffin, R. G. Lipid Dynamics and Protein-Lipid Interactions in 2D Crystals Formed with the B-Barrel Integral Membrane Protein VDAC1. *J. Am. Chem. Soc.* **2012**, *134*, 6375−6387.
(13) Fitzpatrick, A. W. P.; Debelouchina, G. T.; Bayro, M. J.; Clare, D. K.; Caporini, M. A.; Bajaj, V. S.; Jaroniec, C. P.; Wang, L.; Ladizhansky, V.; Mueller, S. A.; et al. Atomic Structure and Hierarchical Assembly of a Cross-β Amyloid Fibril. *Proc. Natl. Acad. Sci. U.S.A.* **2013**, *110*, 5468−5473.
(14) Jaroniec, C. P.; MacPhee, C. E.; Bajaj, V. S.; McMahon, M. T.; Dobson, C. M.; Griffin, R. G. High Resolution Molecular Structure of a Peptide in an Amyloid Fibril Determined by MAS NMR Spectroscopy. *Proc. Natl. Acad. Sci. U.S.A.* **2004**, *101*, 711−716.
(15) Linser, R.; Dasari, M.; Hiller, M.; Higman, V.; Fink, U.; Amo, J.-M. L. d.; Markovic, S.; Handel, L.; Kessler, B.; Schmieder, P.; et al. Proton-Detected Solid-State NMR Spectroscopy of Fibrillar and Membrane Proteins. *Angew. Chem., Int. Ed.* **2011**, *50*, 4508−4512.
(16) Petkova, A. T.; Ishii, Y.; Balbach, J. J.; Antzutkin, O. N.; Leapman, R. D.; Delaglio, F.; Tycko, R. Structural Model for Alzheimer's beta-Amyloid Fibrils Based on Experimental Constraints from Solid State NMR. *Proc. Natl. Acad. Sci. U.S.A.* **2002**, *99*, 16742−16747.
(17) Tycko, R. Progress Towards a Molecular-Level Structural Understanding of Amyloid Fibrils. *Curr. Opin. Struct. Biol.* **2004**, *14* (1), 96−103.
(18) Reif, B.; Jaroniec, C. P.; Rienstra, C. M.; Hohwy, M.; Griffin, R. G. H-1-H-1 MAS Correlation Spectroscopy and Distance Measurements in a Deuterated Peptide. *J. Magn. Reson.* **2001**, *151* (2), 320−327.
(19) Zhou, D. H.; Graesser, D. T.; Franks, W. T.; Rienstra, C. M. Sensitivity and Resolution in Proton Solid-State NMR at Intermediate Deuteration Levels: Quantitative Linewidth Characterization and Applications to Correlation Spectroscopy. *J. Magn. Reson.* **2006**, *178* (2), 297−307.
(20) Lewandowski, J. R.; Dumez, J.-N.; Akbey, U.; Lange, S.; Emsley, L.; Oschkinat, H. Enhanced Resolution and Coherence Lifetimes in the Solid-State NMR Spectroscopy of Perdeuterated Proteins under Ultrafast Magic Angle Spinning. *J. Phys. Chem. Lett.* **2011**, *2*, 2205−2211.
(21) Reif, B. Ultra-high Resolution in MAS Solid-State NMR of Perdeuterated Proteins: Implications for Structure and Dynamics. *J. Magn. Reson.* **2012**, *216*, 1−12.
(22) Harris, R. K.; Becker, E. D. NMR Nomenclature: Nuclear Spin Properties and Conventions for Chemical Shifts-IUPAC Recommendations. *J. Magn. Reson.* **2002**, *156*, 323−326.
(23) Wu, G. Oxygen 17 NMR Studies of Organic and Biological Molecules. *eMagRes*; John Wiley & Sons, Ltd: Chichester, West Sussex, U.K., 2007.
(24) Degroot, H. J. M.; Harbison, G. S.; Herzfeld, J.; Griffin, R. G. Nuclear Magnetic Resonance Study of the Schiff-Base in Bacteriorhodopsin - Counterion Effects on the N-15 Shift Anisotropy. *Biochemistry* **1989**, *28* (8), 3346−3353.
(25) Harbison, G.; Herzfeld, J.; Griffin, R. G. N-15 Chemical-Shift Tensors in L-Histidine Hydrochloride Monohydrate. *J. Am. Chem. Soc.* **1981**, *103* (16), 4752−4754.
(26) Munowitz, M.; Bachovchin, W. W.; Herzfeld, J.; Dobson, C. M.; Griffin, R. G. Acid-Base and Tautomeric Equilibria in the Solid-State - N-15 Nmr-Spectroscopy of Histidine and Imidazole. *J. Am. Chem. Soc.* **1982**, *104* (5), 1192−1196.
(27) Mackenzie, K. J. D.; Smith, M. E. *Multinuclear Solid-State NMR of Inorganic Materials*; Pergamon: London, 2002; Vol. *6*, p 727.
(28) Wu, G. Solid-State 17O NMR Studies of Organic and Biological Molecules. *Prog. Nucl. Magn. Reson. Spectrosc.* **2008**, *52*, 118−169.
(29) Prasad, S.; Clark, T. M.; Sharma, R.; Kwak, H. T.; Grandinetti, P. J.; Zimmermann, H. A Combined O-17 RAPT and MQ-MAS NMR Study of L-Leucine. *Solid State Nucl. Magn. Reson.* **2006**, *29* (1−3), 119−124.
(30) Brinkmann, A.; Kentgens, A. P. M. Proton-Selective $^{17}O-^{1}H$ Distance Measurements in Fast Magic-Angle-Spinning Solid-State NMR Spectroscopy for the Determination of Hydrogen Bond Lengths. *J. Am. Chem. Soc.* **2006**, *128* (46), 14758−14759.
(31) Chemlka, B.; Mueller, K.; Pines, A.; Stebbins, J.; Wu, Y.; Zwanziger, J. O-17 NMR in Solids by Dynamic-Angle Spinning and Double Rotation. *Nature* **1989**, *339*, 42−43.
(32) Baltisberger, J. H.; Gann, S. L.; Grandinetti, P. J.; Pines, A. Cross-Polarization Dynamic-Angle Spinning Nuclear Magnetic Resonance of Quadrupolar Nuclei. *Mol. Phys.* **1994**, *81*, 1109.
(33) Frydman, L.; Harwood, J. S. Isotropic Spectra of Half-Integer Quadrupolar Spins from Bidimensional Magic-Angle Spinning NMR. *J. Am. Chem. Soc.* **1995**, *117*, 5367−5368.
(34) Gan, Z. Satellite Transition Magic Angle Spinning. *J. Am. Chem. Soc.* **2000**, *122*, 3242.
(35) Wu, G.; Rovnyak, D.; Griffin, R. G. Quantitative Multiple-Quantum Magic-Angle-Spinning NMR Spectroscopy of Quadrupolar Nuclei in Solids. *J. Am. Chem. Soc.* **1996**, *118* (39), 9326−9332.
(36) Wu, G.; Rovnyak, D.; Huang, P. C.; Griffin, R. G. High-Resolution Oxygen-17 NMR Spectroscopy of Solids by Multiple-Quantum Magic-Angle-Spinning. *Chem. Phys. Lett.* **1997**, *277* (1−3), 79−83.
(37) Brinkmann, A.; Kentgens, A. P. M. Sensitivity Enhancement and Heteronuclear Distance Measurements in Biological 17O Solid-State NMR. *J. Phys. Chem. B* **2006**, *110* (32), 16089−16101.
(38) Gullion, T.; Yamauchi, K.; Okonogi, M.; Asakura, T. 13C-17O REAPDOR NMR as a Tool for Determining Secondary Structure in Polyamides. *Macromolecules* **2007**, *40* (5), 1363.
(39) Hung, I.; Uldry, A.-C.; Becker-Baldus, J.; Webber, A. L.; Wong, A.; Smith, M. E.; Joyce, S. A.; Yates, J. R.; Pickard, C. J.; Dupree, R.; et al. Probing Heteronuclear 15N-17O and 13C-17O Connectivities and Proximities by Solid-State NMR Spectroscopy. *J. Am. Chem. Soc.* **2009**, *131* (5), 1820−1834.
(40) Sefzik, T. H.; Houseknecht, J. B.; Clark, T. M.; Prasad, S.; Lowary, T. L.; Gan, Z.; Grandinetti, P. J. Solid-State 17O NMR in Carbohydrates. *Chem. Phys. Lett.* **2007**, *434* (4−6), 312−315.
(41) Wong, A.; Beevers, A. J.; Kukol, A.; Dupree, R.; Smith, M. E. Solid-State 17O NMR Spectroscopy Of A Phospholemman Transmembrane Domain Protein: Implications For The Limits Of Detecting Dilute 17O Sites In Biomaterials. *Solid State Nucl. Magn. Reson.* **2008**, *33* (4), 72.
(42) Wu, G.; Dong, S.; Ida, R.; Reen, N. A Solid-State 17O Nuclear Magnetic Resonance Study Of Nucleic Acid Bases. *J. Am. Chem. Soc.* **2002**, *124* (8), 1768.
(43) Yamauchi, K.; Okonogi, M.; Kurosu, H.; Tansho, M.; Shimizu, T.; Gullion, T.; Asakura, T. High Field 17O Solid-State NMR Study of Alanine Tripeptides. *J. Magn. Reson.* **2008**, *190* (2), 327.
(44) Zhu, J.; Ye, E.; Terskikh, V.; Wu, G. Solid-State 17O NMR Spectroscopy of Large Protein-Ligand Complexes. *Angew. Chem., Int. Ed.* **2010**, *49* (45), 8399−8402.
(45) O'Dell, L. A.; Ratcliffe, C. I.; Kong, X.; Wu, G. Multinuclear Solid-State Nuclear Magnetic Resonance and Density Functional Theory Characterization of Interaction Tensors in Taurine. *J. Phys. Chem. A* **2012**, *116* (3), 1008−1014.
(46) Wong, A.; Howes, A. P.; Yates, J. R.; Watts, A.; Anupold, T.; Past, J.; Samoson, A.; Dupree, R.; Smith, M. E. Ultra-High Resolution 17O Solid-State NMR Spectroscopy of Biomolecules: A Comprehensive Spectral Analysis of Monosodium L-Glutamate Monohydrate. *Phys. Chem. Chem. Phys.* **2011**, *13* (26), 12213−12224.

(47) Becerra, L. R.; Gerfen, G. J.; Temkin, R. J.; Singel, D. J.; Griffin, R. G. Dynamic Nuclear Polarization with a Cyclotron Resonance Maser at 5 T. *Phys. Rev. Lett.* **1993**, *71* (21), 3561−3564.
(48) Carver, T. R.; Slichter, C. P. Polarization of Nuclear Spins in Metals. *Phys. Rev.* **1953**, *92*, 212−213.
(49) Gerfen, G. J.; Becerra, L. R.; Hall, D. A.; Griffin, R. G.; Temkin, R. J.; Singel, D. J. High Frequency (140 GHz) Dynamic Nuclear Polarization: Polarization Transfer to a Solute in Frozen Aqueous Solution. *J. Chem. Phys.* **1995**, *102* (24), 9494−9497.
(50) Overhauser, A. W. Polarization of Nuclei in Metals. *Phys. Rev.* **1953**, *92*, 411−415.
(51) Song, C.; Hu, K.-N.; Joo, C.-G.; Swager, T. M.; Griffin, R. G. TOTAPOL − A Biradical Polarizing Agent for Dynamic Nuclear Polarization Experiments in Aqueous Media. *J. Am. Chem. Soc.* **2006**, *128*, 11385−11390.
(52) Dane, E. L.; Corzilius, B.; Rizzato, E.; Stocker, P.; Ouari, O.; Maly, T.; Smith, A. A.; Griffin, R. G.; Ouari, O.; Tordo, P.; et al. Rigid Orthogonal bis-TEMPO Biradicals with Improved Solubility for Dynamic Nuclear Polarization. *J. Org. Chem.* **2012**, *77*, 1789−1797.
(53) Kiesewetter, M.; Corzilius, B.; Smith, A. A.; Griffin, R. G.; Swager, T. M. Dynamic Nuclear Polarization with a Water-soluble Rigid Biradical. *J. Am. Chem. Soc.* **2012**, *134*, 4537−4540.
(54) Matsuki, Y.; Maly, T.; Ouari, O.; Lyubenova, S.; Herzfeld, J.; Prisner, T.; Tordo, P.; Griffin, R. G. Dynamic Nuclear Polarization using a Rigid Biradical. *Angew. Chem.* **2009**, *48*, 4996−5000.
(55) Zagdoun, A.; Casano, G.; Ouari, O.; Lapadula, G.; Rossini, A. J.; Lelli, M.; Baffert, M.; Gajan, D.; Veyre, L.; Maas, W. E.; et al. A Slowly Relaxing Rigid Biradical for Efficient Dynamic Nuclear Polarization Surface-Enhanced NMR Spectroscopy: Expeditious Characterization of Functional Group Manipulation in Hybrid Materials. *J. Am. Chem. Soc.* **2012**, *134*, 2284−2291.
(56) Zagdoun, A.; Casano, G.; Ouari, O.; Schwarzwälder, M.; Rossini, A. J.; Aussenac, F.; Yulikov, M.; Jeschke, G.; Copéret, C.; Lesage, A.; et al. Large Molecular Weight Nitroxide Biradicals Providing Efficient Dynamic Nuclear Polarization at Temperatures up to 200 K. *J. Am. Chem. Soc.* **2013**, *135* (34), 12790−12797.
(57) Hall, D. A.; Maus, D. C.; Gerfen, G. J.; Inati, S. J.; Becerra, L. R.; Dahlquist, F. W.; Griffin, R. G. Polarized-Enhanced NMR Spectroscopy of Biomolecules in Frozen Solution. *Science* **1997**, *276* (5314), 930−932.
(58) Rosay, M.; Lansing, J. C.; Haddad, K. C.; Bachovchin, W. W.; Herzfeld, J.; Temkin, R. J.; Griffin, R. G. High-Frequency Dynamic Nuclear Polarization in MAS Spectra of Membrane and Soluble Proteins. *J. Am. Chem. Soc.* **2003**, *125* (45), 13626−13627.
(59) Rosay, M.; Tometich, L.; Pawsey, S.; Bader, R.; Schauwecker, R.; Blank, M.; Borchard, P. M.; Cauffman, S. R.; Felch, K. L.; Weber, R. T.; et al. Solid-State Dynamic Nuclear Polarization at 263 GHz: Spectrometer Design and Experimental Results. *Phys. Chem. Chem. Phys.* **2010**, *12* (22), 5850−5860.
(60) Rosay, M.; Weis, V.; Kreischer, K. E.; Temkin, R. J.; Griffin, R. G. Two-Dimensional 13C-13C Correlation Spectroscopy with Magic Angle Spinning and Dynamic Nuclear Polarization. *J. Am. Chem. Soc.* **2002**, *124* (13), 3214−3215.
(61) Rosay, M.; Zeri, A. C.; Astrof, N. S.; Opella, S. J.; Herzfeld, J.; Griffin, R. G. Sensitivity-Enhanced NMR Of Biological Solids: Dynamic Nuclear Polarization Of Y21M Fd Bacteriophage And Purple Membrane. *J. Am. Chem. Soc.* **2001**, *123* (5), 1010−1011.
(62) Akbey, U.; Franks, W. T.; Linden, A.; Lange, S.; Griffin, R. G.; van, R. B.-J.; Oschkinat, H. Dynamic Nuclear Polarization of Deuterated Proteins. *Angew. Chem., Int. Ed.* **2010**, *49* (42), 7803−7806.
(63) Bayro, M. J.; Debelouchina, G. T.; Eddy, M. T.; Birkett, N. R.; MacPhee, C. E.; Rosay, M.; Maas, W. E.; Dobson, C. M.; Griffin, R. G. Intermolecular Structure Determination of Amyloid Fibrils with Magic-Angle Spinning and Dynamic Nuclear Polarization NMR. *J. Am. Chem. Soc.* **2011**, *133* (35), 13967−13974.
(64) Debelouchina, G. T.; Bayro, M. J.; van, d. W. P. C. A.; Caporini, M. A.; Barnes, A. B.; Rosay, M.; Maas, W. E.; Griffin, R. G. Dynamic Nuclear Polarization-Enhanced Solid-State NMR Spectroscopy of GNNQQNY Nanocrystals and Amyloid Fibrils. *Phys. Chem. Chem. Phys.* **2010**, *12* (22), 5911−5919.
(65) Lelli, M.; Gajan, D.; Lesage, A.; Caporini, M. A.; Vitzthum, V.; Mieville, P.; Heroguel, F.; Rascon, F.; Roussey, A.; Thieuleux, C.; et al. Fast Characterization of Functionalized Silica Materials by Silicon-29 Surface-Enhanced NMR Spectroscopy using Dynamic Nuclear Polarization. *J. Am. Chem. Soc.* **2011**, *133* (7), 2104−2107.
(66) Mak-Jurkauskas, M. L.; Bajaj, V. S.; Hornstein, M. K.; Belenky, M.; Griffin, R. G.; Herzfeld, J. Energy Transformations Early in the Bacteriorhodopsin Photocycle Revealed by DNP-Enhanced Solid-State NMR. *Proc. Natl. Acad. Sci. U.S.A.* **2008**, *105* (3), 883−888.
(67) Van der Wel, P. C. A.; Hu, K.-N.; Lewandowski, J.; Griffin, R. G. Dynamic Nuclear Polarization of Amyloidogenic Peptide Nanocrystals: GNNQQNY, a Core Segment of the Yeast Prion Protein Sup35p. *J. Am. Chem. Soc.* **2006**, *128* (33), 10840−10846.
(68) Lafon, O.; Thankamony, A. S. L.; Kobayashi, T.; Carnevale, D.; Vitzthum, V.; Slowing, I. I.; Kandel, K.; Vezin, H.; Amoureux, J.-P.; Bodenhausen, G.; et al. Mesoporous Silica Nanoparticles Loaded with Surfactant: Low Temperature Magic Angle Spinning 13C and 29Si NMR Enhanced by Dynamic Nuclear Polarization. *J. Phys. Chem. C* **2012**, *117* (3), 1375−1382.
(69) Takahashi, H.; Ayala, I.; Bardet, M.; De Paëpe, G.; Simorre, J.-P.; Hediger, S. Solid-State NMR on Bacterial Cells: Selective Cell Wall Signal Enhancement and Resolution Improvement using Dynamic Nuclear Polarization. *J. Am. Chem. Soc.* **2013**, *135* (13), 5105−5110.
(70) Ravera, E.; Corzilius, B.; Michaelis, V. K.; Rosa, C.; Griffin, R. G.; Luchinat, C.; Bertini, I. Dynamic Nuclear Polarization of Sedimented Solutes. *J. Am. Chem. Soc.* **2013**, *135* (5), 1641−1644.
(71) Gelis, I.; Vitzthum, V.; Dhimole, N.; Caporini, M.; Schedlbauer, A.; Carnevale, D.; Connell, S.; Fucini, P.; Bodenhausen, G. Solid-State NMR Enhanced by Dynamic Nuclear Polarization as a Novel Tool for Ribosome Structural Biology. *J. Biomol. NMR* **2013**, *56* (2), 85−93.
(72) Lesage, A.; Lelli, M.; Gajan, D.; Caporini, M. A.; Vitzthum, V.; Mieville, P.; Alauzun, J.; Roussey, A.; Thieuleux, C.; Medhi, A.; et al. Surface Enhanced NMR Spectroscopy by Dynamic Nuclear Polarization. *J. Am. Chem. Soc.* **2010**, *132*, 15459−14461.
(73) Ong, T.-C.; Mak-Jurkauskas, M. L.; Walish, J. J.; Michaelis, V. K.; Corzilius, B.; Smith, A. A.; Clausen, A. M.; Cheetham, J. C.; Swager, T. M.; Griffin, R. G. Solvent-Free Dynamic Nuclear Polarization of Amorphous and Crystalline ortho-Terphenyl. *J. Phys. Chem. B* **2013**, *117* (10), 3040−3046.
(74) Potapov, A.; Yau, W.-M.; Tycko, R. Dynamic Nuclear Polarization-Enhanced 13C NMR Spectroscopy of Static Biological Solids. *J. Magn. Reson.* **2013**, *231* (0), 5−14.
(75) Rossini, A. J.; Zagdoun, A.; Hegner, F.; Schwarzwälder, M.; Gajan, D.; Copéret, C.; Lesage, A.; Emsley, L. Dynamic Nuclear Polarization NMR Spectroscopy of Microcrystalline Solids. *J. Am. Chem. Soc.* **2012**, *134* (40), 16899−16908.
(76) Takahashi, H.; Hediger, S.; De Paepe, G. Matrix-Free Dynamic Nuclear Polarization Enables Solid-State NMR 13C-13C Correlation Spectroscopy of Proteins at Natural Isotopic Abundance. *Chem. Commun.* **2013**, *49*, 9479−9481.
(77) Maly, T.; Andreas, L. B.; Smith, A. A.; Griffin, R. G. 2H-DNP-Enhanced 2H-13C Solid-State NMR Correlation Spectroscopy. *Phys. Chem. Chem. Phys.* **2010**, *12* (22), 5872−5878.
(78) Michaelis, V. K.; Markhasin, E.; Daviso, E.; Herzfeld, J.; Griffin, R. G. Dynamic Nuclear Polarization of Oxygen-17. *J. Phys. Chem. Lett.* **2012**, *3*, 2030−2034.
(79) Vitzthum, V.; Caporini, M. A.; Bodenhausen, G. Solid-State Nitrogen-14 Nuclear Magnetic Resonance Enhanced by Dynamic Nuclear Polarization using a Gyrotron. *J. Magn. Reson.* **2010**, *205*, 177−179.
(80) Vitzthum, V.; Mieville, P.; Carnevale, D.; Caporini, M. A.; Gajan, D.; Coperet, C.; Lelli, M.; Zagdoun, A.; Rossini, A. J.; Lesage, A. Dynamic Nuclear Polarization of Quadrupolar Nuclei using Cross Polarization from Protons: Surface-Enhanced Aluminium-27 NMR. *Chem. Commun.* **2012**, *48* (14), 1988−1990.
(81) Lee, D.; Takahashi, H.; Thankamony, A. S. L.; Dacquin, J. P.; Bardet, M.; Lafon, O.; De Paepe, G. Enhanced Solid-State NMR

Correlation Spectroscopy of Quadrupolar Nuclei using Dynamic Nuclear Polarization. *J. Am. Chem. Soc.* **2012**, *134* (45), 18491−18494.
(82) Blanc, F.; Sperrin, L.; Jefferson, D. A.; Pawsey, S.; Rosay, M.; Grey, C. P. Dynamic Nuclear Polarization Enhanced Natural Abundance 17O Spectroscopy. *J. Am. Chem. Soc.* **2013**, *135* (8), 2975−2978.
(83) Lafon, O.; Rosay, M.; Aussenac, F.; Lu, X.; Trebosc, J.; Cristini, O.; Kinowski, C.; Touati, N.; Vezin, H.; Amoureux, J.-P. Beyond the Silica Surface by Direct Silicon-29 Dynamic Nuclear Polarization. *Angew. Chem.* **2011**, *50* (36), 8367−8370.
(84) Lafon, O.; Thankamony, A. S. L.; Rosay, M.; Aussenac, F.; Lu, X.; Trebosc, J.; Bout-Roumazeilles, V.; Vezin, H.; Amoureux, J.-P. Indirect and Direct 29Si Dynamic Nuclear Polarization of Dispersed Nanoparticles. *Chem. Commun.* **2013**, *49* (28), 2864−2866.
(85) Maly, T.; Miller, A. F.; Griffin, R. G. In Situ High-Field Dynamic Nuclear Polarization-Direct and Indirect Polarization of C-13 Nuclei. *ChemPhysChem* **2010**, *11* (5), 999−1001.
(86) Michaelis, V. K.; Smith, A. A.; Corzilius, B.; Haze, O.; Swager, T. M.; Griffin, R. G. High-Field 13C Dynamic Nuclear Polarization with a Radical Mixture. *J. Am. Chem. Soc.* **2013**, *135* (8), 2935−2938.
(87) Wind, R. A.; Duijvestijn, M. J.; Vanderlugt, C.; Manenschijn, A.; Vriend, J. Applications of Dynamic Nuclear-Polarization in C-13 NMR in Solids. *Prog. Nucl. Magn. Reson. Spectrosc.* **1985**, *17*, 33−67.
(88) Hu, K.-N.; Iuga, D.; Griffin, R. G. In *DNP enhanced 17O SSNMR Spectroscopy on Biological Solids*, Experimental NMR Conference, Asilomar, CA, 2003; p 317.
(89) Michaelis, V. K.; Markhasin, E.; Daviso, E.; Corzilius, B.; Smith, A.; Herzfeld, J.; Griffin, R. G. In *DNP NMR of Oxygen-17 using Mono- and Bi-radical Polarizing Agents.*, Experimental NMR Conference, Miami, FL, 2012.
(90) Corzilius, B.; Smith, A. A.; Barnes, A. B.; Luchinat, C.; Bertini, I.; Griffin, R. G. High-Field Dynamic Nuclear Polarization with High-Spin Transition Metal Ions. *J. Am. Chem. Soc.* **2011**, *133*, 5648−5651.
(91) Hu, K.; Bajaj, V.; Rosay, M.; Griffin, R. High-Frequency Dynamic Nuclear Polarization using Mixtures of TEMPO and Trityl Radicals. *J. Chem. Phys.* **2007**, *126* (4), 044512-7.
(92) Hwang, C. F.; Hill, D. A. Phenomenological Model for New Effect in Dynamic Polarization. *Phys. Rev. Lett.* **1967**, *19*, 1011−1014.
(93) Kessenikh, A. V.; Lushchikov, V. I.; Manenkov, A. A.; Taran, Y. V. Proton Polarization in Irradiated Polyethylenes. *Sov. Phys. Solid State* **1963**, *5*, 321−329.
(94) Maly, T.; Debelouchina, G. T.; Bajaj, V. S.; Hu, K. N.; Joo, C. G.; Mak-Jurkauskas, M. L.; Sirigiri, J. R.; van der Wel, P. C. A.; Herzfeld, J.; Temkin, R. J.; et al. Dynamic Nuclear Polarization at High Magnetic Fields. *J. Chem. Phys.* **2008**, *128* (5), 052211-19.
(95) Wollan, D. S. Dynamic Nuclear-Polarization with an Inhomogeneously Broadened ESR Line. 1. Theory. *Phys. Rev. B* **1976**, *13* (9), 3671−3685.
(96) Wollan, D. S. Dynamic Nuclear-Polarization with an Inhomogeneously Broadened ESR Line. 2. Experiment. *Phys. Rev. B* **1976**, *13* (9), 3686−3696.
(97) Abragam, A. *Principles of Nuclear Magnetic Resonance*; Oxford University Press: New York, 1961.
(98) Slichter, C. P. *Principles of Magnetic Resonance*; Harper & Row: New York, 1963.
(99) Taulelle, F. *NMR of Quadrupolar Nuclei in the Solid State*; Kluwer Academic Publishers: London, 1988; Vol. *322*, p 476.
(100) Lemaitre, V.; Smith, M. E.; Watts, A. A Review of Oxygen-17 Solid-State NMR of Organic Materials - Towards Biological Applications. *Solid State Nucl. Magn. Reson.* **2004**, *26* (3−4), 215−235.
(101) Pike, K. J.; Lemaitre, V.; Kukol, A.; Anupold, T.; Samoson, A.; Howes, A. P.; Watts, A.; Smith, M. E.; Dupree, R. Solid-State 17O NMR of Amino Acids. *J. Phys. Chem. B* **2004**, *108* (26), 9256−9263.
(102) Wu, G. Oxygen 17 NMR Studies of Organic and Biological Molecules. *Encyclopedia of Magnetic Resonance*; John Wiley & Sons, Ltd.: Chichester, West Sussex, U.K., 2011.
(103) Ashbrook, S. E.; Wimperis, S. Quadrupolar Coupling: An Introduction and Crystallographic Aspects. *eMagRes*; John Wiley & Sons, Ltd: Chichester, West Sussex, U.K., 2007.
(104) Fernandez, C.; Pruski, M. Probing Quadrupolar Nuclei by Solid-State NMR Spectroscopy: Recent Advances. *Top. Curr. Chem.* **2012**, *306*, 119−188.
(105) Man, P. P. *Encyclopedia of Analytical Chemistry*; John Wiley and Sons: Chichester, U.K., 2000; pp 12224−12265.
(106) Dong, S.; Ida, R.; Wu, G. A Combined Experimental and Theoretical 17O NMR Study of Crystalline Urea: An Example of Large Hydrogen-Bonding Effects. *J. Phys. Chem. A* **2000**, *104*, 11194−11202.
(107) Woskov, P. W.; Bajaj, V. S.; Hornstein, M. K.; Temkin, R. J.; Griffin, R. G. Corrugated Waveguide and Directional Coupler for CW 250 GHz Gyrotron DNP Experiments. *IEEE Trans. Microwave Theory Tech.* **2005**, *53*, 1863−1869.
(108) Becerra, L. R.; Gerfen, G. J.; Bellew, B. F.; Bryant, J. A.; Hall, D. A.; Inati, S. J.; Weber, R. T.; Un, S.; Prisner, T. F.; McDermott, A. E.; et al. A Spectrometer for Dynamic Nuclear-Polarization and Electron- Paramagnetic-Resonance at High-Frequencies. *J. Magn. Reson., Ser. A* **1995**, *117* (1), 28−40.
(109) Barnes, A. B.; Mak-Jurkauskas, M. L.; Matsuki, Y.; Bajaj, V. S.; Wel, P. C. A. v. d.; DeRocher, R.; Bryant, J.; Sirigiri, J. R.; Temkin, R. J.; Lugtenburg, J.; et al. Cryogenic sample exchange NMR probe for magic angle spinning dynamic nuclear polarization. *J. Magn. Reson.* **2009**, *198*, 261−270.
(110) Daviso, E.; Diller, A.; Alia, A.; Matysik, J.; Jeschke, G. Photo-CIDNP MAS NMR Beyond the T(1) Limit by Fast Cycles of Polarization Extinction and Polarization Generation. *J. Magn. Reson.* **2008**, *190* (1), 43−51.
(111) Pons, M.; Feliz, M.; Giralt, E. Steady-State DQF-COSY Spectra Using a Variable Relaxation Delay. *J. Magn. Reson.* **1988**, *78*, 314−320.
(112) Veshtort, M.; Griffin, R. G. Spinevolution: A Powerful Tool for the Simulation of the Solid and Liquid State NMR Experiments. *J. Magn. Reson.* **2006**, *178* (2), 248−282.
(113) Eichele, K. *WSolids NMR Simulation Package*, 1.20.21; 2013.
(114) Davis, J. H.; Jeffrey, K. R.; Bloom, M.; Valic, M. I.; Higgs, T. P. Quadrupolar Echo Deuteron Magnetic Resonance Spectroscopy in Ordered Hydrocarbon Chains. *Chem. Phys. Lett.* **1976**, *42* (2), 390−394.
(115) Rhodes, H. E.; Wang, P. K.; Stokes, H. T.; Slichter, C. P.; Sinfelt, J. H. NMR of Platinum Catalysts. 1 Line Shapes. *Phys. Rev. B* **1982**, *26* (7), 3559−3568.
(116) Massiot, D.; Farnan, I.; Gautier, N.; Trumeau, D.; Trokiner, A.; Coutures, J. P. Ga-71 and Ga-69 Nuclear Magnetic Resonance Study of Beta-Ga2O3 Resolution of 4-fold and 6-fold Coordinated Ga Sites in Static Conditions. *Solid State Nucl. Magn. Reson.* **1995**, *4* (4), 241−248.
(117) Bernal, J. D.; Fowler, R. H. A Theory of Water and Ionic Solution, with Particular Reference to Hydrogen and Hydroxyl Ions. *J. Chem. Phys.* **1933**, *1*, 515−548.
(118) Sklar, N.; Senko, M. E.; Post, B. Thermal Effects in Urea - Crystal Structure at −140 degrees C and at Room Temperature. *Acta Crystallogr.* **1961**, *14*, 716−720.
(119) Scheringer, C. Die Kristallstruktur des Phenols. *Z. Kristallogr.* **1963**, *119*, 273−283.
(120) Clark, S. J.; Segall, M. D.; Pickard, C. J.; Hasnip, P. J.; Probert, M. J.; Refson, K.; Payne, M. C. First Principles Methods using CASTEP. *Z. Kristallogr.* **2005**, *220* (5−6), 567−570.
(121) Perdew, J. P.; Burke, K.; Ernzerhof, M. Generalized Gradient Approximation Made Simple. *Phys. Rev. Lett.* **1996**, *77*, 3865−3868.
(122) Perdew, J. P.; Burke, K.; Ernzerhof, M. Generalized Gradient Approximation Made Simple - Reply. *Phys. Rev. Lett.* **1998**, *80*, 891−891.
(123) Vanderbilt, D. Soft Self-Consistent Pseudopotentials In A Generalized Eigenvalue Formalism. *Phys. Rev. B* **1990**, *41* (11), 7892−7895.
(124) Profeta, M.; Mauri, F.; Pickard, C. J. Accurate First Principles Predication of 17O NMR Parameters in SiO2: Assignment of the Zeolite Ferrierite Spectrum. *J. Am. Chem. Soc.* **2003**, *125*, 541−548.

(125) Yates, J. R.; Pickard, C. J.; Mauri, F. Calculation of NMR Chemical Shifts for Extended Systems using Ultrasoft Pseudopotentials. *Phys. Rev. B* **2007**, *76*, 024401-11.
(126) Yates, J. R.; Pickard, C. J.; Payne, M. C.; Dupree, R.; Profeta, M.; Mauri, F. Theoretical Investigation of Oxygen-17 NMR Shielding and Electric Field Gradients in Glutamic Acid Polymorphs. *J. Phys. Chem. A* **2004**, *108*, 6032−6037.
(127) Haze, O.; Corzilius, B.; Smith, A. A.; Griffin, R. G.; Swager, T. M. Water−Soluble Narrow Line Radicals for Dynamic Nuclear Polarization. *J. Am. Chem. Soc.* **2012**, *134*, 14287−14290.
(128) Thaning, M. Free Radicals, U.S. Patent 6,013,810, 2000.
(129) Barnes, A. B.; De Paepe, G.; van der Wel, P. C. A.; Hu, K. N.; Joo, C. G.; Bajaj, V. S.; Mak-Jurkauskas, M. L.; Sirigiri, J. R.; Herzfeld, J.; Temkin, R. J.; et al. High-Field Dynamic Nuclear Polarization for Solid and Solution Biological NMR. *Appl. Magn. Reson.* **2008**, *34* (3−4), 237−263.
(130) Hu, K.-N.; Yu, H.-H.; Swager, T. M.; Griffin, R. G. Dynamic Nuclear Polarization with Biradicals. *J. Am. Chem. Soc.* **2004**, *126* (35), 10844−10845.
(131) Smith, A. A.; Corzilius, B.; Barnes, A. B.; Maly, T.; Griffin, R. G. Solid Effect Dynamic Nuclear Polarization and Polarization Pathways. *J. Chem. Phys.* **2012**, *136*, 015101-1−015101-16.
(132) Corzilius, B.; Andreas, L. B.; Smith, A. A.; Ni, Q. Z.; Griffin, R. G. Paramagnet Induced Signal Quenching in MAS-DNP Experiments on Homogeneous Solutions. *J. Magn. Reson.* **2013**, submitted for publication.
(133) Corzilius, B.; Smith, A. A.; Griffin, R. G. Solid Effect in Magic Angle Spinning Dynamic Nuclear Polarization. *J. Chem. Phys.* **2012**, *137*, 054201-12.
(134) Salzmann, C. G.; Radaelli, P. G.; Hallbrucker, A.; Mayer, E.; Finney, J. L. The Preparation and Structures of Hydrogen Ordered Phases of Ice. *Science* **2006**, *311* (5768), 1758−1761.
(135) Spiess, H. W.; Garrett, B. B.; Sheline, R. K. Oxygen-17 Quarupole Coupling Parameters for Water in its Various Phases. *J. Chem. Phys.* **1969**, *51* (3), 1201−1205.
(136) Ba, Y.; Ripmeester, J. A.; Ratcliffe, C. I. Water Molecular Reorientation in Ice and Tetrahydrofuran Clathrate Hydrate from Lineshape Analysis of 17O Spin-Echo NMR Spectra. *Can. J. Chem.* **2011**, *89*, 1055−1064.
(137) Antzutkin, O. N.; Iuga, D.; Filippov, A. V.; Kelly, R. T.; Becker-Baldus, J.; Brown, S. P.; Dupree, R. Hydrogen Bonding in Alzheimer's Amyloid-β Fibrils Probed by 15N{17O} REAPDOR Solid-State NMR Spectroscopy. *Angew. Chem., Int. Ed.* **2012**, *51* (41), 10289−10292.
(138) Stringfellow, T. C.; Farrar, T. C. Temperature Dependence of the 14N Quadrupole Coupling Constant of Isocyanomethane. *J. Chem. Phys.* **1995**, *102* (24), 9465−9473.
(139) Lucken, E. A. C. *Nuclear Quadrupole Coupling Constants*; Academic: London, 1969.
(140) Zhu, J.; Lau, J. Y. C.; Wu, G. A Solid-State 17O NMR Study of L-Tyrosine in Different Ionization States: Implications for Probing Tyrosine Side Chains in Proteins. *J. Phys. Chem. B* **2010**, *114*, 11681−11688.
(141) Herzfeld, J.; Berger, A. E. Sideband Intensitites in NMR-Spectra of Samples Spinning at the Magic Angle. *J. Chem. Phys.* **1980**, *73* (12), 6021−6030.
(142) Harris, R. K.; Wasylishen, R. E.; Duer, M. J. *NMR Crystallography*, 1st ed.; John Wiley & Sons: Chichester, West Sussex, U.K., 2009.